Hamiltonian dynamics and the phase transition of the *XY* model

Xavier Leoncini and Alberto D. Verga*
Institut de Recherche sur les Phénomènes Hors Equilibre,† 12, Avenue Général Leclerc, F-13003 Marseille, France

Stefano Ruffo
Dipartimento di Energetica ''S. Stecco,'' Università degli Studi di Firenze, INFN and INFM, Via di Santa Marta, 3 50139 Firenze, Italy
(Received 1 December 1997)

A Hamiltonian dynamics is defined for the *XY* model by adding a kinetic energy term. Thermodynamical properties (total energy, magnetization, vorticity) derived from microcanonical simulations of this model are found to be in agreement with canonical Monte Carlo results in the explored temperature region. The behavior of the magnetization and energy as functions of the temperature are thoroughly investigated, taking into account finite size effects. By representing the spin field as a superposition of random phased waves, we derive a nonlinear dispersion relation whose solutions allow the computation of thermodynamical quantities, which agree quantitatively with those obtained in numerical experiments, up to temperatures close to the transition. At low temperatures the propagation of phonons is the dominant phenomenon, while above the phase transition the system splits into ordered domains separated by interfaces populated by topological defects. In the high temperature phase, spins rotate, and an analogy with an Ising-like system can be established, leading to a theoretical prediction of the critical temperature $T_{KT} \approx 0.855$. [S1063-651X(98)15205-4]

PACS number(s): 05.20.−y, 64.60.Cn

I. INTRODUCTION

The two dimensional *XY* model, also known as the planar spin model, presents many interesting behaviors. Despite the presence of a continuous symmetry group, a particular form of phase transition exists [1,2], which can be characterized by the change in the behavior of the correlation functions. In the low temperature phase these latter have power law decay, showing that the system is in a long range order state; while they decay exponentially at high temperatures, the long range order is broken, even though thermodynamic quantities remain smooth across the transition [3]. These observations have been interpreted by Kosterlitz and Thouless [4] using an analogy with the transition of a Coulomb gas from a dielectric phase, where charges are bounded into dipoles, to a plasma (conducting) phase where temperature fluctuations destroy the dipoles, and the charges become free. In the *XY* system the charges are replaced by topological excitations called vortices.

From the analytical point of view, beyond the spin-wave approximation [5], and the Villain model [6], the use of the renormalization group in the critical region has been the main issue [7,8]. In order to confirm the analytical results and to satisfy the need for a better understanding of the transition, many numerical studies have been performed. Different dynamics, like Monte Carlo [9] or Langevin [10], have been introduced. The system has been confirmed to be dominated by spin-wave excitations in the low temperature region. The transition region is then determined using the information on the correlation functions, and is interpreted in terms of dipole unbinding. However, there is a number of observations in the literature that seems to complicate this simple picture of the phase transition mechanism. Among the different results, those worth mentioning are the visualization of the vortex distribution [9], the presence of domains delimited by topological defects [10], and the precise determination of the transition temperature $T_{KT} \approx 0.89$ [11], much lower than the transition temperature of the Villain model. Results are also found on the interaction between vortices [10], or the vortex interaction energy [12].

Although the basic mechanism of the Kosterlitz-Thouless transition, in terms of the breaking of vortex dipoles associated with the emergence of a disordered state, is well understood, the observation of the spatial distribution of defects, which is not uniform (defects tend to appear organized into clusters at temperatures slightly larger than the transition temperature), and the presence of large ordered domains where the spins are almost parallel, seem to indicate that the physics of the phase transition is not exhausted by this unbinding process but that some kind of partial local order is present even beyond the transition temperature. The investigation of the system properties near the transition is one of the points addressed in this paper.

On the other hand, the question of whether statistical physics is able to describe, over a wide range of temperatures, the behavior of a classical Hamiltonian system with many degrees of freedom, still remains an open one (see, e.g., the literature on the Fermi-Pasta-Ulam model quoted in Ref. [13]). Therefore, it seemed interesting to consider the *XY* model from the point of view of Hamiltonian dynamical systems by adding a kinetic energy term to the *XY* Hamiltonian. Such an approach has proved to provide interesting information on typical relaxation time scales and collective behaviors in the one-dimensional (1D) case [14] and in the mean field approximation [15]. More recently Lyapunov ex-

*Electronic address: verga@marius.univ-mrs.fr
†Unité Mixte de Recherche 6594, Center National de la Recherche Scientifique, Universités d'Aix-Marseille I et II.

ponents have been computed, confirming the presence of long relaxation times to equilibrium both in the very low and very high temperature limits in one dimension [16], and the presence of a change in slope of the maximal Lyapunov exponent vs the energy near the transition temperature in two dimensions [17] (also see also Ref. [18] for a preliminary study of this latter phenomenon).

The present model is one of the coupled rotators (spins) sitting on the sites of a square lattice interacting with near neighbors, whose statistical properties are described by the microcanonical ensemble, the total energy being set by the initial conditions. Convergence to a Gibbsian equilibrium distribution is not taken for granted in the whole temperature range on accessible time scales. Therefore, particular attention must be devoted to the temporal behavior of the different quantities which characterize macroscopic thermodynamical properties. One notices, however, that the spatial topology is unchanged, and that the existence of a continuous symmetry group of rotation is also maintained in the dynamics. This implies that a Kosterlitz-Thouless-type transition must be observed (in the thermodynamic limit) with typically strong finite size effects, like the existence of a nonzero magnetization [5,19].

In this paper we concentrate on a study of those properties of the dynamics of the XY model which reproduce equilibrium features, postponing to a future work the study of nonequilibrium effects. We anticipate that we are able to reproduce most of the equilibrium behaviors of macroscopic quantities, which makes microcanonical dynamics competitive with canonical Monte Carlo, since here we do not have to extract random numbers, stochasticity being supplied by the intrinsic chaoticity of the model.

The fact that we actually deal with a dynamical system allows us to develop an original analytical approach to the study of the thermodynamics, which is based on the approximate solution of the equations of motion. This method is based upon the ergodic properties of the dynamics and on the separation of temporal scales present in the spin motion.

In Sec. II we present the Hamiltonian model and the basic aspects of the numerical computations, and we introduce the thermodynamic and dynamical quantities that characterize the state of the system. In Sec. III we compare the statistical properties of our model to the usual ones, using both analytical and numerical approaches. We derive the thermodynamical properties using the hypothesis that the dynamics is dominated by random phased waves. We then propose, in Sec. IV, an Ising-like model based on the observation that, above the transition, synchronized regions of spins appear. The relation of XY to an Ising-like model allows us to describe the high temperature phase and to derive an approximate value of the critical temperature. A brief summary of the main results and conclusions is presented in Sec. V.

II. HAMILTONIAN MODEL, BASIC PROPERTIES AND NUMERICAL COMPUTATIONS

The XY model was introduced in statistical mechanics as a two-dimensional version of the Heisenberg Hamiltonian. The spins are fixed on the sites of a square lattice, and are characterized by a rotation angle $\theta_i \in [-\pi, \pi]$,

$$H_{XY} = J \sum_{(i,j)}^{N} [1 - \cos(\theta_i - \theta_j)], \tag{2.1}$$

where J is the coupling constant (with $J>0$ corresponding to the ferromagnetic case, that we study here), and i and j label the N sites of a square lattice of side $\sqrt{N}$, i.e., $i=(i_x,i_y)$, with $1 \leqslant i_x, i_y \leqslant \sqrt{N}$ of coordinates (x,y). The summation is extended over all i and its neighboring sites j. In the following, without loss of generality, we set $J=1$, and the lattice step equal to unity.

The spins evolve in time, $\theta_i = \theta_i(t)$, after adding a kinetic energy term to the XY Hamiltonian,

$$H = \sum_{i=1}^{N} \frac{p_i^2}{2} + H_{XY}, \tag{2.2}$$

where $p_i = \dot{\theta}_i$ is the spin momentum. The choice $J=1$ is equivalent to setting time units and to rescaling momentum accordingly (in these units the ''inertia'' is also unity). With this kinetic energy term the spins in fact become rotators, and the XY model becomes a system of coupled rotators. The equations of motion are

$$\ddot{\theta}_i(t) = -\sum_{j(i)}^{4} \sin[\theta_i(t) - \theta_j(t)], \tag{2.3}$$

where the summation is over the four neighbors j of site i. In addition to the energy $H=E$, there exists a second constant of the motion, the total angular momentum $P = \Sigma_i p_i$, which can be chosen to be zero. We choose periodic boundary conditions in both the x and y directions. Numerical integration of Eq. (2.3) is performed using the Verlet algorithm, which conserves the energy $O(\Delta t^2)$, Δt being the time step, but exactly preserves momentum and the symplectic structure.

Thermodynamical quantities are computed by averaging over time and over the sites of a single orbit (the evolution of the system from a given initial condition). Typically, the system is started with a Gaussian distribution of momenta and with all the spins pointing in the same direction $\theta_i = \theta_0$, for reasons that are clarified in the following. No strong dependence on the chosen initial condition in this class was observed, but one could statistically improve our results by averaging over many orbits with different initial conditions and the same energy.

The temperature is computed through the average squared momentum per spin,

$$T = \frac{1}{N} \sum_{i=1}^{N} \overline{p_i(t)^2}, \tag{2.4}$$

where the overbar stands for temporal averaging.

The thermodynamical state can be characterized by several macroscopic variables: the internal energy per spin $h = h(T) = E(T,N)/N$ (E being the constant total energy of the system); the magnetization $\mathbf{M} = \mathbf{M}(T,N)$, which, as mentioned in Sec. I vanishes for $N \to \infty$, but is sizable for any finite N; and the density of topological defects ρ_v, or vortices, which is intimately related to the mechanism underlying the phase transition.

The magnetization $\mathbf{M} = (M_x, M_y)$ is given by

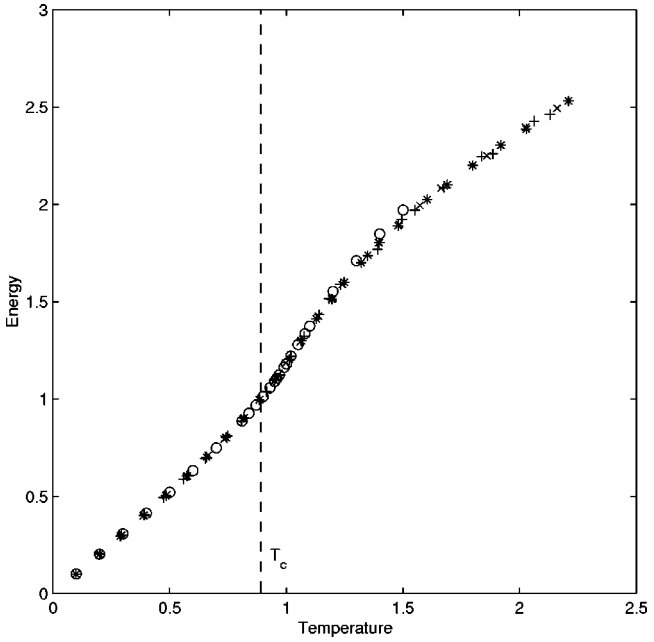

FIG. 1. Total energy per spin as a function of the temperature. At low temperature the energy grows as T, and at high temperature the energy tends to $T/2+2$. The Kosterlitz-Thouless phase transition occurs at $T_{\mathrm{KT}}\approx 0.89$; $+$, $\times$, and * signs refer to the Hamiltonian dynamical simulations for different lattice sizes, $N=64^2$, $N=128^2$, and $N=256^2$ respectively; and circles refer to canonical Monte Carlo simulations for a lattice size of $N=100^2$.

$$\mathbf{M}\equiv\overline{\mathbf{M}(t)}=\frac{1}{N}\sum_{i=1}^{N}\left(\overline{\cos\,\theta_i},\overline{\sin\,\theta_i}\right), \tag{2.5}$$

and describe the mean orientation of the spin field. A topological defect is identified, as usual, by computing the total angle circulation on a given plaquette (the sum of the four plaquette relative angles $\mathrm{mod}[-\pi,\pi]$); when it equals $\pm 2\pi$, this quantity identifies a positive (negative) unitary vortex on the plaquette. The total density of vortices, or vorticity, which is an intensive quantity, is then given by

$$\rho_v=\frac{1}{N}\sum_{[i,j]}\left(\theta_{j+1}-\theta_j\right)\ \mathrm{mod}[-\pi,\pi], \tag{2.6}$$

where $[i,j]$ denotes the sites j of the ith plaquette. We have studied the temporal evolution and spatial distribution of the vortices as a function of the temperature. Because of the periodic boundary conditions, and since $P=0$, the number of positive vortices equals the number of negative ones.

We have performed simulations using various sets of parameters, to study the system behavior depending on the temperature, the number of spins, and the total time to test the stationarity of the relaxed state. Having chosen parallel spins, one has an initially vanishing potential energy, allowing the exploration of the low temperature region through the reduction of kinetic energy. Random angles in the $[-\pi,\pi]$ interval would give an energy per spin of 2, which would then remain fixed producing a high temperature configuration, as can also be deduced from the $h(T)$ function we compute below (see Fig. 1). Therefore, initially, the magnetization is $|\mathbf{M}|=1$. Other initial conditions, with $|\mathbf{M}|=0$ were investigated, for instance, with half the spins oriented in the x direction, and the other half in the $-x$ direction. After a transient, the system relaxes to the same thermodynamical state.

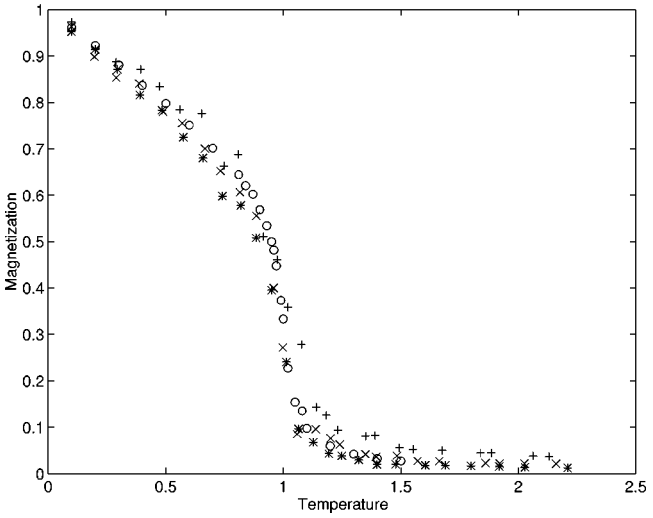

FIG. 2. Absolute value of the magnetization as a function of the temperature. Finite size effects give a finite magnetization at low temperatures. At low temperatures the magnetization decreases only logarithmically with the number of spins. $+$, $\times$, and * signs refer to the Hamiltonian dynamical simulations for different lattice sizes $N=64^2$, $N=128^2$, and $N=256^2$ respectively; and circles refer to Monte Carlo simulations for a lattice size of $N=100^2$.

In Fig. 1, we plot the total energy per spin $h(T)$. The low ($T\ll 1$, $T\approx 1$ corresponds to the value for which the kinetic energy is of the same order of the potential energy) and high ($T\gg 1$) temperature behaviors are easy to understand. At low temperature equipartition of kinetic and potential energies gives $h(T)\approx T$ (this is the linear regime, where angles between neighboring spins are small). At high temperature, angles are uniformly distributed in $[-\pi,\pi]$, the cosine interaction in Eq. (2.2) is negligible with respect to the kinetic energy, and then $h(T)\approx T/2+2$. These simple arguments suggest that for $T\ll 1$, the spin field is almost linear, and can be represented as a superposition of waves, which correspond to phonons; while, for $T\gg 1$, the potential energy is negligible, and this field becomes a set of almost free fast rotators. The change in the behavior of the $h(T)$ curve starts around the Kosterlitz-Thouless critical temperature T_{KT}. The peak in the specific heat, related to the second derivative of the energy, occurs instead at a somewhat higher temperature, a fact well documented in Monte Carlo computations.

Figure 2 shows the absolute value of the magnetization as measured using formula (2.5). Although in the thermodynamic limit the magnetization must vanish, in a finite system and for low temperature we expect an observable macroscopic magnetization, which decreases logarithmically with the number of spins, as noted by Berezinskii [3]. This slow decrease with system size is hardly observable in Fig. 2, but points corresponding to larger sizes systematically give a smaller magnetization. In the high temperature region, since angles are randomly distributed in space at any time, the magnetization vanishes algebraically with the number of spins.

The behavior of vorticity with temperature, plotted in Fig.

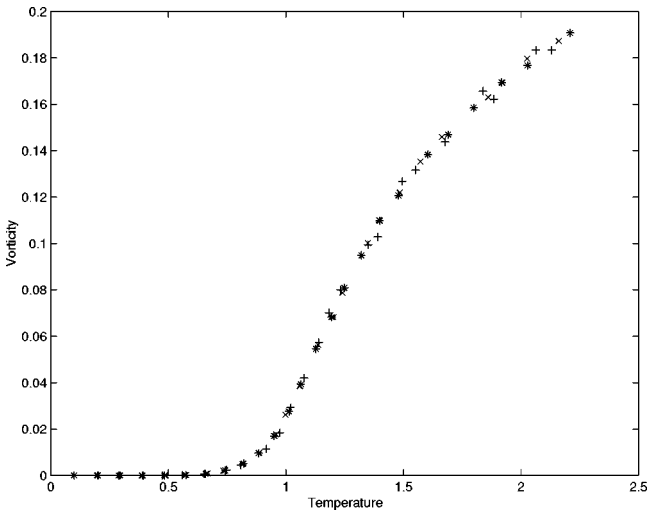

FIG. 3. Number density of vortices as a function of the temperature normalized to the total number of spins. This quantity is intensive. +, ×, and * signs refer to the Hamiltonian dynamical simulations for different lattice sizes $N=64^2$, $N=128^2$, and $N=256^2$, respectively.

3, is related to the form of the $h(T)$ curve. Indeed, at low temperature, aligned angle configurations are typical, and consequently vorticity vanishes, $\rho_v \to 0$. In the high temperature regime, spins are randomly distributed and the vortex density approaches the asymptotic value $\rho_v \to \frac{1}{3}$. A dramatic growth of the vorticity occurs in the phase transition region (the temperature in the range $T \approx 0.8-1.5$).

All our results are in perfect agreement with those of Monte Carlo simulations (see, e.g., Ref. [20]); some of them are plotted in Figs. 1 and 2 for comparison. Therefore, microcanonical (Hamiltonian dynamics) and canonical (Monte Carlo) computations give, at least for the class of initial conditions studied here, the same thermodynamical equilibrium states.

III. DYNAMICAL AND STATISTICAL PROPERTIES

We know that, at low temperatures, the main contribution to the canonical partition function comes from the configurations in which the spins are almost aligned, configurations where the angle differences $\theta_i - \theta_j$ are small. In such a situation, the equations of motion (2.3) can be linearized, and the spin field is therefore represented as a superposition of linear waves. Here we will determine the effective dispersion relation for these waves at low temperature using consistency relations with temperature and internal energy. Let us introduce a representation of the spin angles in the form of a random phased field,

$$\theta_i = \sum_k \alpha_k \cos(\psi_k^i), \quad \psi_k^i = k x_i - \omega_k t + \phi_k, \qquad (3.1)$$

where the summation is over the wave vectors $k=(k_x,k_y) = 2\pi(n_x,n_y)/\sqrt{N}$, with $n_x,n_y = 1,\ldots,\sqrt{N}$ integers; the wave spectrum is given by α_k, and the phases ϕ_k are supposed to be random, uniformly distributed in the circle. We also should add to Eq. (3.1) a term of the form $\Omega_i t$ reflecting the individual rotation of spins with some frequency Ω_i, which in fact can be considered a function of the temperature. However, at low temperature most of these frequencies must vanish, because the energy needed to trigger the free rotation is only reached at energies of the order of $h=2$ (or temperatures of the order of $T=1.5$, as can be seen in Fig. 1), when a spin, considered as a perturbed pendulum, crosses the separatrix. In the following we set $\Omega_i = 0$ at low temperature (this term becomes important at high temperatures).

Although the main assumption in Eq. (3.1), that is, the random character of the wave phases, may only be justified *a posteriori*, we performed some numerical tests which showed that this ansatz is consistent with the properties of the system (at low and also at finite temperatures). We found that the probability distribution of the spin velocities is almost uniform, and that, moreover, the motion of one single spin is ergodic (in the sense that its temporal mean and variance coincide with the spatial ones). In addition, if the system were linear, this assumption is equivalent to the assumption of thermodynamic equilibrium (with a bath at temperature T). In fact this is the case at very low and very high T; of course, in the intermediate range the influence of the nonlinearity becomes important, for instance, establishing nonlocal interactions or some type of self-organization, in which case this assumption would not necessarily be valid.

In formula (3.1), there are two unknown functions of the wave number which remain to be determined: the wave frequencies ω_k and the spectrum α_k. Note, in addition, that Eq. (3.1) is in fact a change of variables of the angles θ_i to the amplitudes α_k, where, implicitly, a slow temporal dependence may be included, the fast time dependence being assured by the phase $\omega_k t$. In this sense, formula (3.1) is rather general, and can take into account a large variety of field states.

The definition of the temperature imposes a constraint on the form of the wave spectrum. Indeed, substituting formula (3.1) into the definition of the temperature (2.4), we obtain

$$T = \frac{1}{N}\sum_i^N \langle \dot{\theta}_i^2 \rangle = \tfrac{1}{2} \sum_k \alpha_k^2 \omega_k^2, \qquad (3.2)$$

where $\langle \cdots \rangle$ stands for averaging over the random phases ϕ_k, and where we used the identity

$$\langle \cos(\psi_k^i)\cos(\psi_{k'}^i) \rangle = \tfrac{1}{2}\,\delta_{k,k'},$$

$\delta_{k,k'}$ being the Kronecker symbol. For instance, if equipartition of the energy among different degrees of freedom is assumed, one obtains the usual Jeans spectrum, given by

$$\alpha_k^2 = \frac{2T}{N\omega_k^2}, \qquad (3.3)$$

which means that each degree of freedom takes a fraction $T/2$ of the total kinetic energy. In fact, as we will show below, a detailed knowledge of the spectrum turns out not to be necessary to derive the dispersion relation and compute thermodynamical quantities.

Before proceeding to the computation of the dispersion relation, let us derive a general expression of the energy per spin h,

$$h=\frac{T}{2}+2-\frac{1}{N}\sum_{(i,j)}^{N}\langle\cos(\theta_i-\theta_j)\rangle, \tag{3.4}$$

where the first term comes from the definition of the temperature; the second term is the constant added for convenience to the Hamiltonian to make the energy vanish at zero temperature; and the last term includes, for each lattice site, a summation over two neighbors, for instance west (in the x direction) and south (in the y direction). When expansion (3.1) is introduced into Eq. (3.4), the typical contribution to the sum in the third term on the right hand side is

$$U_N^{(i,j)}=\left\langle \cos\left[\sum_{n=1}^{N} A_{k_n}^{(i,j)}\sin(B_{k_n}(i,j)+\phi_{k_n})\right]\right\rangle,$$

where n relabel the modes, and

$$A_{k_n}^{(i,j)}=2\sin\left[\frac{k\cdot(x_i-x_j)}{2}\right],$$

$$B_{k_n}^{(i,j)}=\frac{k\cdot(x_i+x_j)}{2}+\omega_k t$$

are local in n and independent on the phases ϕ_{k_n}. Let us split the summation over the wave numbers into two terms: one containing the phase ϕ_{k_N} and the other with the remaining $n=1,\ldots,N-1$ phases. Since

$$\begin{aligned}\langle\cos[A_{k_N}^{(i,j)}\sin(B_{k_N}^{(i,j)}+\phi_{k_N})]\rangle&=J_0(A_{k_N}^{(i,j)}),\\ \langle\sin[A_{k_N}^{(i,j)}\sin(B_{k_N}^{(i,j)}+\phi_{k_N})]\rangle&=0,\end{aligned} \tag{3.5}$$

where J_0 is the Bessel function of zero order, we obtain the recursion relation

$$U_N^{(i,j)}=J_0(A_{k_N}^{(i,j)})U_{N-1}^{(i,j)},$$

which readily gives the result

$$U_N^{(i,j)}=\prod_n J_0(A_{k_n}^{(i,j)}).$$

We finally obtain

$$h=\frac{T}{2}+2-\prod_k J_0(\beta_x)-\prod_k J_0(\beta_y), \tag{3.6}$$

where $\beta_x=2\alpha_k\sin k_x/2$ and $\beta_y=2\alpha_k\sin k_y/2$, and the last two products come from north (south) and east (west) neighbors on the lattice. Equation (3.6) is the general expression for the energy per spin, as long as the system is dominated by random phased waves. We note that in the case of a symmetric spectrum $\alpha_{k_x,k_y}=\alpha_{k_y,k_x}$ (this is the case for the Jeans spectrum, when the dispersion relation satisfies $\omega_{k_x,k_y}=\omega_{k_y,k_x}$), the products of zero order Bessel functions are equal,

$$\frac{v}{2}=\prod_k J_0(\beta_x)=\prod_k J_0(\beta_y), \tag{3.7}$$

where v is related to h by $h(T)=T/2+2-v(T)$, and is the average potential energy. In order to obtain an explicit form of the energy per spin as a function of the temperature, $h=h(T)$, we must determine in a self-consistent way the dispersion relation; this may be done by using the equation of motion in its full nonlinear form. But let us begin with the linear case, which will serve as a guide to the self-consistent computation. The linear equation of motion reads

$$\ddot{\theta}_i=\sum_{\langle j\rangle}\theta_i-\theta_j. \tag{3.8}$$

Substituting Eq. (3.1), one obtains

$$\begin{aligned}-\sum_k \omega_k^2\alpha_k\cos\psi_k^i&\\ &=-\sum_k \beta_x\left[\sin\left(\psi_k^i+\frac{k_x}{2}\right)-\sin\left(\psi_k^i-\frac{k_x}{2}\right)\right]\\ &\quad-\sum_k \beta_y\left[\sin\left(\psi_k^i+\frac{k_y}{2}\right)-\sin\left(\psi_k^i-\frac{k_y}{2}\right)\right]\\ &=-4\sum_k \alpha_k\left[\sin^2\left(\frac{k_x}{2}\right)+\sin^2\left(\frac{k_y}{2}\right)\right]\cos\psi_k^i,\end{aligned} \tag{3.9}$$

although the linearity of the equation allows an identification term by term in the summation over k, a different strategy for the solution would be to average Eq. (3.9) over all the phases but one, e.g., over the phases $\phi_{k'}\neq\phi_k$ after multiplying both sides by $\cos\psi_k^i$, in order to isolate only one term in the summation on the left hand side. One finally obtains the linear dispersion relation

$$\omega_k=\omega_{0k}=4\left(\sin^2\frac{k_x}{2}+\sin^2\frac{k_y}{2}\right). \tag{3.10}$$

The frequency spectrum is symmetric with respect to the exchange $k_x\leftrightarrow k_y$; in the following we assume, without loss of generality, that the spectrum is symmetric with respect to this transformation.

This procedure can be generalized to the nonlinear case, although the right hand side of Eq. (2.3) is no longer local in ϕ_k. After substituting expansion (3.1) into Eq. (2.3), we must average over the phases $\phi_{k'}\neq\phi_k$, which we denote $\langle\cdots\rangle'$, terms of the form

$$\langle\sin(\theta-\theta_E)\rangle'=-\left\langle\sin\left[\sum_k \beta_x\sin\left(\psi_k+\frac{k_x}{2}\right)\right]\right\rangle', \tag{3.11}$$

where θ_E is, e.g., the east neighbor of angle θ, having a phase $\psi_E=\psi_k+k_x=kx+k_x-\omega_k t+\phi_k$. We now split the summation in Eq. (3.11) into a term containing the phase ϕ_k and others, and develop the sine of the summation of two terms into a product. The averaging of these two terms reduces to

$$\left\langle\cos\left[\sum_{k'} \beta_x\sin\left(\psi_k'\pm\frac{k_x'}{2}\right)\right]\right\rangle'=\frac{v}{2J_0(\beta_x)}, \tag{3.12}$$

because the averaging of the sine term is zero. The two neighbors in the x direction (west and east sites) give the following expression:

$$\langle \sin(\theta-\theta_E)\rangle' + \langle \sin(\theta-\theta_W)\rangle' = -\frac{v}{2J_0(\beta_x)}\left\{\sin\left[\beta_x \sin\left(\psi_k+\frac{k_x}{2}\right)\right] - \sin\left[\beta_x \sin\left(\psi_k-\frac{k_x}{2}\right)\right]\right\}. \quad (3.13)$$

Those in the y direction give exactly the same contribution, with $\beta_x \to \beta_y$. On the other hand, the left hand side of Eq. (2.3), the temporal part of the equation of motion, is reduced, after substitution of the random wave expression, to

$$\langle \ddot{\theta}_i \rangle = -\omega_k^2 \alpha_k \cos\, \psi_k^i. \quad (3.14)$$

As before, in the linear computation, we multiply both sides of the equations of motion (3.14) and (3.13) (including the similar terms for the north and south neighbors), by $\cos(\psi_k^i)$, and average over the phase ϕ_k, noting that this average involves first order Bessel functions J_1. We finally find the desired dispersion relation

$$\omega_k^2 \alpha_k = 2v\left[\sin\left(\frac{k_x}{2}\right)\frac{J_1(\beta_x)}{J_0(\beta_x)} + \sin\left(\frac{k_y}{2}\right)\frac{J_1(\beta_y)}{J_0(\beta_y)}\right]. \quad (3.15)$$

This dispersion relation is nonlinear, i.e., the frequency depends on the spectrum amplitudes, in two ways: implicitly through the α_k's in v and explicitly in the Bessel functions. To go further, let us investigate the dependence of the arguments of the Bessel functions on the parameters T and N, and the related limiting form of the total energy per spin h. We know that v, being an intensive thermodynamic quantity, does not depend on the number of spins (the size of the system); moreover, the linear frequency (3.10) is bounded from below, $\omega_{0k}^2 \sim \sin^2(k_x/2) > O(1/N)$. We also note, as it is natural for a system near an equilibrium state, that a large number of k modes must contribute to the energy of the system, and then in general we have $\alpha_k^2 \sin k_x/2 \to 0$ when $N \to \infty$, for a large range of temperatures. If this were not the case, the energy would be concentrated in a few high k modes, which is clearly in contrast with the observations. For the Jeans spectrum, one finds specifically $\alpha_k^2 \sin k_x/2 \approx O(T/\sqrt{N})$. Using these approximations, we can now develop the logarithm of the product of the Bessel functions in Eq. (3.7) to obtain

$$v = 2\exp\left\{-\tfrac{1}{8}\sum_k \alpha_k^2 \omega_{0k}^2\right\}. \quad (3.16)$$

In the same approximation, for fixed temperatures and large lattices, the dispersion relation (3.15) reduces to

$$\omega_k^2 = \frac{v\,\omega_{0k}^2}{2}. \quad (3.17)$$

Introducing this expression into formula (3.16) for v, and using the definition of the temperature in terms of random phased waves [Eq. (3.2)], we obtain an implicit equation for the potential energy,

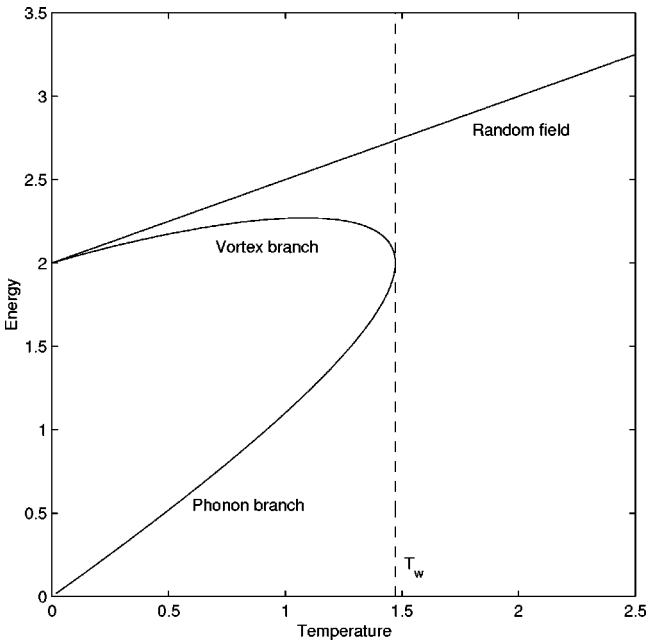

FIG. 4. Plot of the energy density vs temperature computed from Eq. (3.18). The straight line characterizes the random field state, the lower branch the phonons (spin waves), and the upper branch the lattice excitations of the vortex dipole type.

$$v = 2\exp\left[-\frac{T}{2v}\right]. \quad (3.18)$$

We notice that the nonlinear dispersion relation reduces to the linear one for $T=0$. The nonlinear effects, taken into account in Eq. (3.17), appear as a renormalization of the phonon frequency (energy) due to the coupling of the phonons with a thermal bath created by the other phonons as in a mean field. We also note that the factor 2, found in the right hand side of Eq. (3.18) and in the exponent, can be related to the lattice dimensionality (it results from the addition of the x and y terms). Moreover, as we anticipated, formula (3.18) does not depend explicitly on the form of the spectrum α_k.

Let us now investigate the implicit equation (3.18) by solving it numerically. In Fig. 4, where the energy density h versus the temperature T is plotted using formulas $h = T/2 + 2 - v(T)$ and Eq. (3.18), we see three branches according to the solutions of Eq. (3.18). Although the three branches are in principle acceptable solutions, they would have different ''weights.'' For instance, if one associates to each branch a Gibbsian probability, proportional to $\exp(-h_i/T)$, where h_i denotes the branch energy $i=0$, 1, and 2, the lower branch has, at a given temperature, the higher probability. The choice of a Gibbsian probability distribution of states is not in contradiction with our microcanonical approach. Indeed, the energies h_i are related to *macroscopic* equilibrium states, and the Gibbs probabilities represent the best choice, taking into account the usual constraints of maximal entropy and normalization.

The straight line corresponds to the solution $v=0$, which represents a random spin field. Indeed, in the high temperature region, since the potential energy is bounded, we can expect that the rotators are freely rotating without any order,

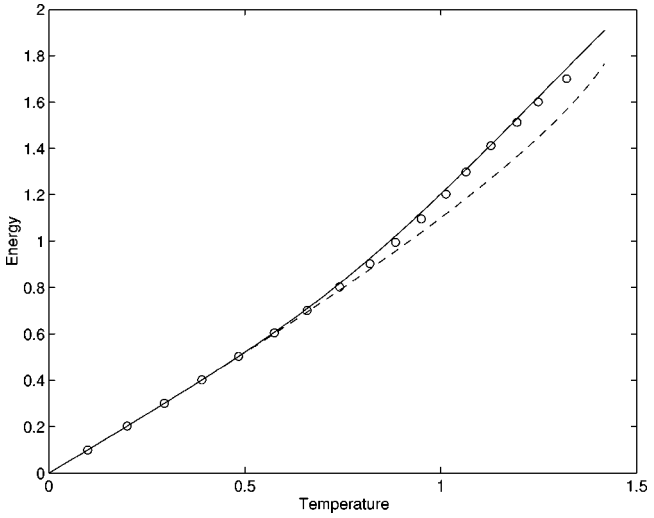

FIG. 5. Plot of the energy density vs the temperature. The circles refer to the numerical data, the dashed line to the phonon branch of Eq. (3.18), and the solid line to the theoretical averaged density of energy [Eq. (3.19)].

i.e., that $(\theta_i-\theta_j)$ is random with constant distribution in $[0, 2\pi)$. This gives us an energy density $h=T/2+2$ and $v(T)=0$. The implicit solution of Eq. (3.18) thus extrapolates the good asymptotic behavior of the energy for high temperature to low temperature regions. This solution exists for any temperature, but in the low temperature region a spin configurations associated with this branch should be unstable (in the sense that for general initial conditions, as in our numerical computations, the system cannot evolve to this state).

Below a certain temperature $T=T_w$, we also see that two other branches appear. As the lower branch has the higher probability, in the low temperature region we may expect the lower energy branch, which we call the phonon branch, to be the physical relevant solution, and the third branch to have no physical meaning at all. However, if we now consider that in fact the lattice is populated with two types of species of different energies $h_1(T)$ and $h_2(T)$ corresponding to the lower (phonons) and upper (which we call vortex) branch, respectively, we obtain

$$h=\frac{h_1 e^{-2h_1/T}+h_2 e^{-2h_2/T}}{e^{-2h_1/T}+e^{-2h_2/T}}, \tag{3.19}$$

which is almost in total agreement with the numerical data up to T_w, as we can see in Fig. 5.

The upper branch can be related to ''dipole vortices,'' since it starts at an energy equal to 2 (see Fig. 4), corresponding to a lattice composed by topological defects forming a perfect crystal [$\theta_i-\theta_j=\pm\pi/2$ and $\Sigma_{j(i)}\sin(\theta_i-\theta_j)=0$ overall the lattice]. This crystal state, which is in fact a periodic array of dipoles, is a stationary solution of the equations of motion at $T=0$, around which no linear development can be made (the linear term is zero, vortices can be considered as nonlinear particles). The factor 2 in the exponents of Eq. (3.19) takes into account that vortices come in pairs (dipoles at low temperature) on the lattice in order to conserve the total circulation.

The temperature T_w determines the upper border of the wave dominated regime; above this temperature the wave branch disappears (as well as the vortex dipole branch). In order to determine T_w, precisely it is useful to rewrite Eq. (3.18) as a formula for the temperature in terms of v,

$$T=-2v\ \ln(v/2). \tag{3.20}$$

If we now calculate the extremum of $T(v)$ for $0<v<2$, we obtain, for $v=2/e=T_w/2$, $T=T_w=4/e\approx 1.47$, which is exactly the critical temperature found in Ref. [21] using a Hartree-Fock approximation. This temperature also appears with the use of renormalization techniques in Ref. [22]. In this case, we note that the equation for v is formally identical to the one for the renormalization constant in this renormalization group calculation. However, the two methods are basically different, and in particular the relation between v and the dispersion relation (3.17), allows us to obtain more precise information on the different thermodynamical quantities of the system. For instance, as mentioned above, the relation between v and h, which is different from the relation between the renormalization constant and the energy, leads to a very good description of the $h(T)$ curve up to T_w.

Let us now evaluate the magnetization for a finite size system with periodic boundaries using the same approach as before: we assume that the spin field can be represented by a superposition of random phased waves (3.1). We call θ_0 the average over the lattice of the θ_i; it is a constant, since the total momentum is conserved. An average of the magnetization over the random phases brings up a calculation similar to the one for the energy per spin, and leads to

$$\langle\mathbf{M}\rangle=\prod_k J_0(\alpha_k)(\cos\ \theta_0,\sin\ \theta_0). \tag{3.21}$$

This expression remains exact as long as the random phase approximation is valid. In order to develop the logarithm of this expression, we have to take into account that $\alpha_k^2<O(T)$, which implies that the development is only valid in the low temperature regimes $T\ll 1$. Moreover a detailed knowledge of the spectrum is also required. Therefore, considering the observed almost flat spectrum of the momentum, we assume the equipartition of the kinetic energy among the modes and use the Jeans spectrum given in Eq. (3.3). The absolute value of the magnetization, $\langle|\mathbf{M}|\rangle$, is given by the product over the different k of the Bessel functions. In the low temperature regime, using Eqs. (3.17) and (3.3), we obtain, for its logarithm,

$$\ln(\langle|\mathbf{M}|\rangle)=-\sum_k\ \frac{\alpha_k^2}{4}=-\frac{T}{2N}\sum_k\ \frac{1}{\omega_k^2}=-\frac{T}{v}G(0), \tag{3.22}$$

where G is the Green function of the linear wave equation, $G(r)=\Sigma_k\exp(ik\cdot r)/\omega_{0k}^2$, with $G(0)=(1/4\pi)\ln(2N)$. The expression for the magnetization is then

$$\langle\mathbf{M}\rangle=\left(\frac{1}{2N}\right)^{T/4\pi v}(\cos\ \theta_0,\sin\ \theta_0). \tag{3.23}$$

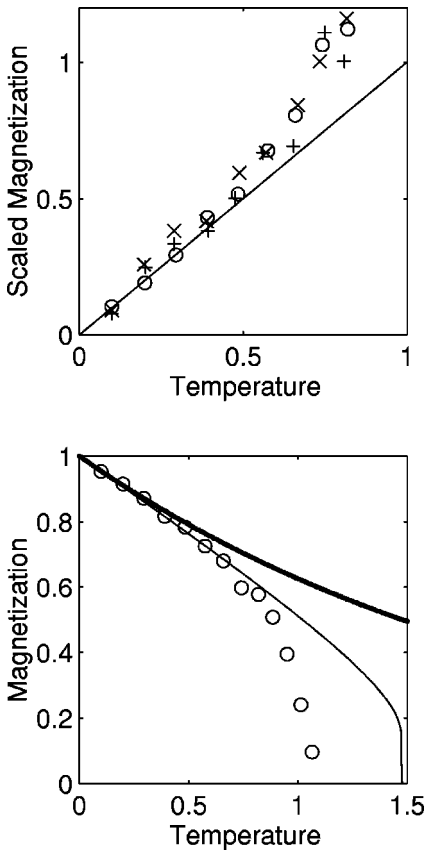

FIG. 6. Finite size effects on the magnetization. The upper plot shows $-4\pi v\ \ln(M)/\ln(2N)$ as a function of the temperature; the line refers to formula (3.23); $+$, $\times$, and $\bigcirc$ refer to numerical data for lattice sizes of $N=64^2$, $N=128^2$, and $N=256^2$, respectively. The lower plot shows $M(T)$; circles are for a $N=256^2$ lattice. The thin line is the analytical result, and the dotted line is the result using only the contribution of linear spin waves: $M=\exp[-T\ \ln(2N)/8\pi]$.

A plot of this expression, scaled in order to obtain a function of the temperature, $-4\pi v\ \ln(M)/\ln(2N)$, is shown in Fig. 6 (top). Within the errors of the numerical data, the points collapse, at low temperature, to a unique curve. Result (3.23), obtained including the correction due to the nonlinear contribution to the dispersion relation, substantially improves the usual estimation based on the linear wave approximation (see the bottom of the figure). The agreement of the theoretical results and the numerical data can be made more precise by taking into account the different energy branches. Indeed, if we now take into account that the lattice is populated by two types of species, we can consider that only the phonons contribute to the magnetization, vortex dipoles having total magnetization zero. As the density of phonons is given by $n_1=e^{-2h_1/T}/(e^{-2h_1/T}+e^{-2h_2/T})$, the observed magnetization must then be simply $n_1\mathbf{M}$. The absolute value of this quantity is plotted in Fig. 6 (bottom). The agreement with numerical data is valid up to the critical temperature.

In the same way we compute the averaged absolute value of the magnetization,

$$\langle|\mathbf{M}|^2\rangle=\frac{1}{N^2}\sum_{i,j}\ \langle\cos(\theta_i-\theta_j)\rangle,$$

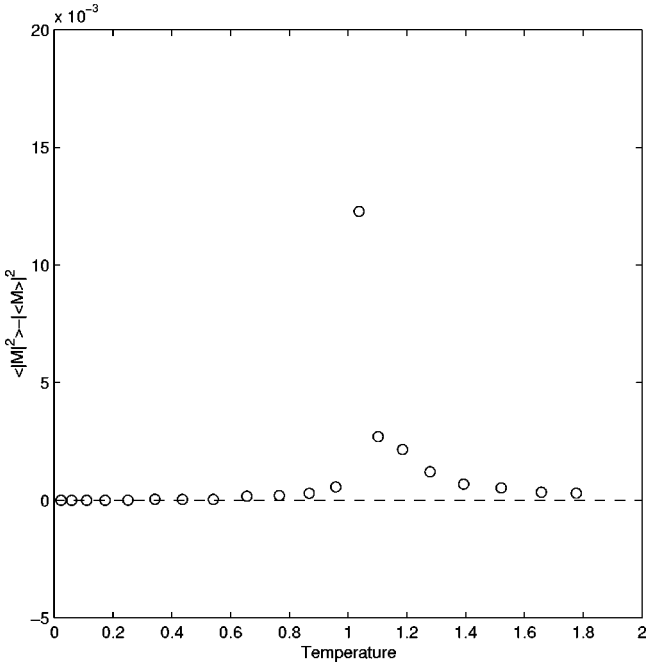

FIG. 7. Plot of the variance of the magnetization vs the temperature ($N=128^2$). The transition region ($T\approx 1$) is clearly identified.

and we obtain the expression

$$\langle|\mathbf{M}|^2\rangle=\frac{1}{N^2}\sum_{i,j}\ \prod_k\ J_0\left[2\alpha_k\sin\left(k\frac{x_i-x_j}{2}\right)\right], \quad (3.24)$$

which, in the low temperature regime, assuming a Jeans spectrum, and making the same expansion as in Eq. (3.22), leads to

$$\langle|\mathbf{M}|^2\rangle=\frac{1}{N^2}\sum_{i,j}\ \exp\left(-\frac{2T}{v}G(r_{ij})\right),$$

where $r_{ij}=x_i-x_j$. A first order calculation leads to the same result as Eq. (3.23), implying that the variance $\mathrm{Var}(\mathbf{M})\equiv\langle|\mathbf{M}|^2\rangle-|\langle\mathbf{M}\rangle|^2$ vanishes at leading order in the temperature. However, at finite temperature, the two values can differ, and the variance of the magnetization can have a nonzero value. This variance can moreover be used to characterize the phase transition, since it is the average over the lattice of the correlation function $\langle e^{\theta_i-\theta_j}\rangle$; it is also related to the susceptibility $\chi\equiv(N/T)\mathrm{Var}(\mathbf{M})$. Indeed, in Fig. 7, we plot the magnetization variance as a function of the temperature, and find that up to temperatures of the order of the Kosterlitz-Thouless T_{KT}, the variance remains very small, and, suddenly, it grows around T_{KT}. This behavior suggests that the magnetization is distributed almost like a δ function, in the low temperature regime (all the spins are pointing to the same direction), and that, near the transition, the amount of randomly oriented spins increases dramatically. Higher order effects on the variance of the magnetization can be computed using the identity

$$J_0(2z\ \sin\ \alpha)=J_0^2(z)+\sum_{m=1}^{\infty}J_m^2(z)\cos(2m\alpha),$$

which gives, after replacing it into Eq. (3.24),

$$\mathrm{Var}(\mathbf{M}) = |\langle \mathbf{M} \rangle|^2 \left(\frac{1}{N^2} \sum_{i,j} \prod_k [1 + M_k(r_{ij})] - 1 \right),$$

where

$$M_k(r_{ij}) = \sum_m \frac{J_m^2(\alpha_k)}{J_0^2(\alpha_k)} \cos(mkr_{ij}).$$

To the first nonvanishing order $(m=1)$, we obtain

$$\mathrm{Var}(\mathbf{M}) = 2 \left(\frac{T}{vN} \right)^2 |\langle \mathbf{M} \rangle|^2 \sum_k \frac{1}{\omega_{0k}^4}.$$

This allows us to compute an approximate value of the susceptibility χ,

$$\chi \approx 3.8710^{-3} \frac{T}{v^2} (2N)^{(1 - T/2\pi v)}.$$

A similar result can be found in Ref. [23], in the limit $v \to 2$.

Concerning the density of vortices, we can see in Fig. 3 that around $T \approx 1.3$ the curve has an inflexion point. This change in the number of defects may be explained as follows. Let us consider a single plaquette. A defect may appear when the four angles are in increasing (decreasing) order, and the last angle is larger (smaller) than $\pi\,(-\pi)$, if the first angle is set to zero. In our model, due to the continuous symmetry group, no particular direction is favored, and therefore the successive differences between the angles $\theta_i - \theta_j$ (discrete gradients) are all equivalent. A defect is then obtained when these gradients satisfy (on average) $\langle |\theta_i - \theta_j| \rangle > \pi/3$. At low temperatures, the amplitudes of the local gradients are determined by the phonons and become steeper at higher temperatures, reaching a point where they are large enough to generate the vortices. Using the previous results, we calculate the temperature for which this condition is reached,

$$\langle (\theta_i - \theta_j)^2 \rangle = 2 \sum_k \alpha_k^2 \sin^2 \frac{k_x}{2} = \frac{T}{v(T)} = \frac{\pi^2}{9}. \quad (3.25)$$

If we now substitute this result into Eq. (3.18), we find

$$T = \frac{2\pi^2}{9} \exp\left(-\frac{\pi^2}{18} \right) \approx 1.27, \quad (3.26)$$

which is in very good agreement with the position of the inflexion point in the numerical data. One may consider that around this temperature a proliferation of vortices should occur.

IV. PHASE TRANSITION

The usual physical picture of the Kosterlitz-Thouless transition is based on the unbinding of vortex pairs: below the critical temperature long range correlations are established by spin waves, the phonons in our Hamiltonian model; above the critical temperature long range order is destroyed by the proliferation of free vortices. This simple physical picture of the mechanism of the transition does not exhaust the complex processes related to the appearance of a kind of self-organization in the system: the vortex distribution is not uniform; vortices form clusters which separate domains of relatively well ordered spins. In this section we study, using numerical simulations, the spatial distribution of topological defects and the equilibrium configurations of the system, using an Ising-like model, in order to describe the partial order which is still present above T_{KT}.

In Sec. III, we showed that the ordered state of the system is dominated by phonons, and that a second type of excitations, the vortex dipoles, is also present. The energies of the two branches meet at a temperature T_w, above which both modes disappear, suggesting that a phase transition to a disordered state might occur. Within this picture, T_w would thus be the temperature where the unbinding of vortex dipoles appears, destroying the long range order created by the waves. However, the actual transition temperature T_{KT} is much lower than T_w, indicating that other processes, not included in the representation (3.1) of the spin motion, take place.

Indeed, in this low temperature analysis we have omitted the rotation of the spin, excluding terms of the form $\Omega_i t$. Moreover, most significantly, we have assumed that the phases of the spin field were random and uncorrelated from site to site, thus neglecting the influence of organized spin motion. Although the proliferation of vortices breaks the long range order, the spin field can still be organized into domains (where the spins rotate synchronously) separated by lines of vortices. The phase transition would be associated in this case, with the appearance of a self-organized state, where, although long range order is absent, a kind of partial local order, established by separated domains of coherent spins, sets in.

We consider this possibility and study the spatial distribution of defects around the critical temperature. By direct visualization of the spin field $\mathbf{m}_i = (\cos\theta_i, \sin\theta_i)$, we noted that the number of isolated defects is negligible, and that they often appear to be in small clusters along the domain borders (this may already be seen in Fig. 7 of Ref. [9]). The problem one encounters with a direct visualization is that the spins move too fast to allow the observation of coherent structures. To gain some further insight, we then introduce a new diagnostic to visualize the spatial structures correctly. We update each spin of the lattice with one fifth of the sum of itself and its four nearest neighbors, and repeat this operation a few times, to obtain an effective local magnetization centered on the considered spin. This local average magnetization is then defined by the iteration

$$\mathbf{m}_i^{(n+1)} = \frac{1}{5} \left[\mathbf{m}_i^{(n)} + \sum_{j(i)}^{4} \mathbf{m}_j^{(n)} \right], \quad n = 1, \ldots, l,$$

where $j(i)$ are the four neighbors of site i, and the number of iterations is typically $l = 10$. The resulting field $\mathbf{m}_i^{(l)}$ is smoother than the initial field $\mathbf{m}_i^{(1)}$; at these temperatures the amplitude of spin motion is large, and it defines a direction at a given site, weighted by the orientation of the surrounding spins.

The effective spin field is shown in Fig. 8. The upper plots are linear gray scale images of the quantity $\sin^2(2\theta_i^{(l)})$

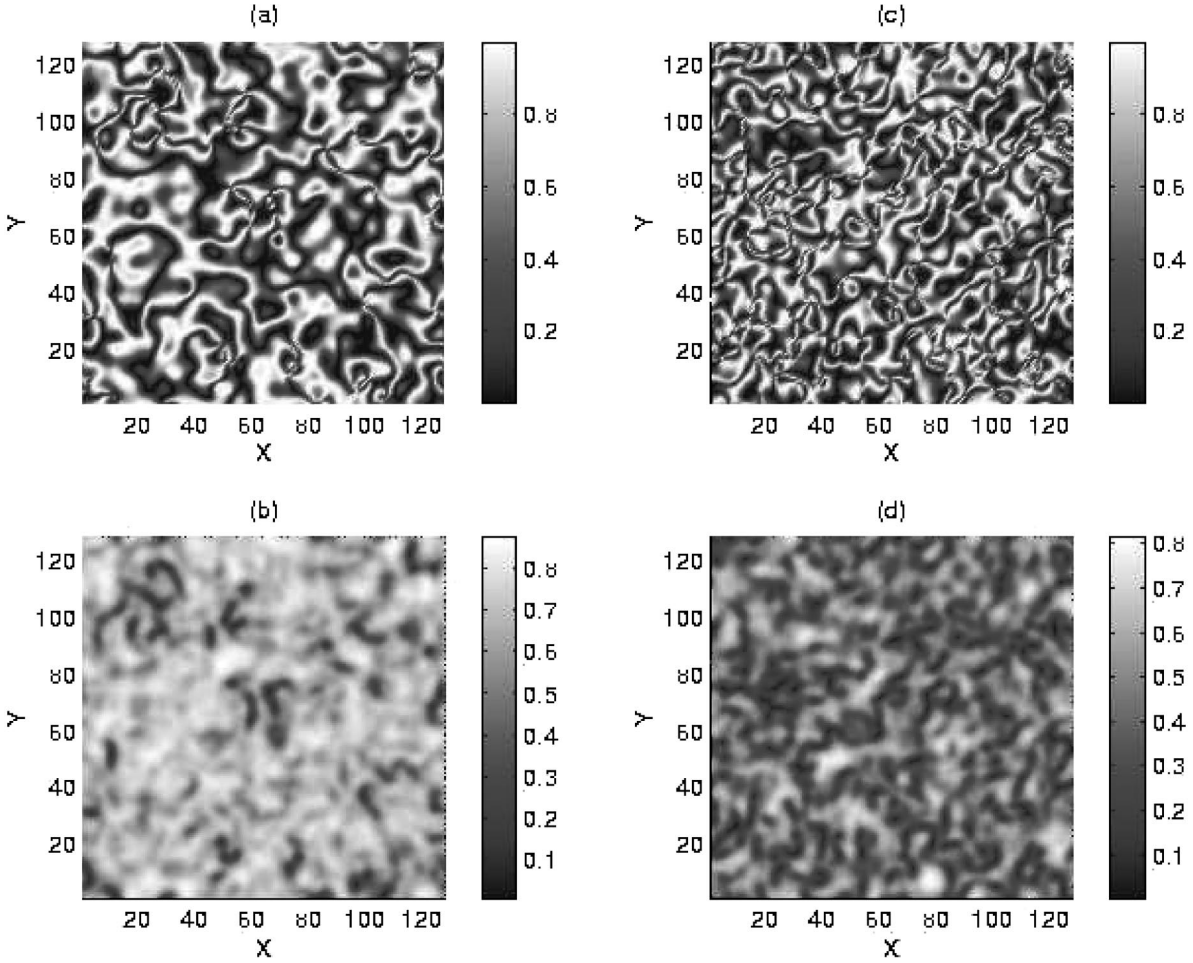

FIG. 8. Spatial distribution of the local magnetization, showing the domains and the interfaces (see text). (a) and (c) Orientation $[\sin^2(\theta_i^l/2)]$; one passes from white to black by a rotation of $\pi/4$. (b) and (d) Intensity ($|\mathbf{m}_i^{(l)}|$); disordered regions are shown in black. (a) and (b) $T=1.02$. (c) and (d) $T=1.29$.

(see also Ref. [10]), where $\theta_i^{(l)}$ is the angle of the local magnetization, and the bottom ones are images of the quantity $|\mathbf{m}_i^{(l)}|$. In the upper plots we can easily locate the vortices by looking at pinching of the darker and brighter areas. They appear to be all bounded in dipoles or chains of dipoles. The presence of these chains can be interpreted as the birth of interfaces separating domains with local order. These latter are more visible in the bottom images, where the brighter regions characterize strong local magnetization, and therefore locally aligned spins; while the darker regions, where the orientation of spins change rapidly with position, indicate the presence of vortex defects and disorder. In the left images, representing a system of $N=128^2$ spins at a temperature slightly above the critical temperature, $T=1.02$, we see that the disordered regions are highly concentrated, and that they tend to connect themselves along lines. This tendency is even more clear in the right images, where we show a system at $T=1.29$. We also note that the size of the ordered regions, the domains, are much smaller at higher temperatures. At $T=1.02$, the domains occupy connected regions of a size comparable to that of the whole system; at higher temperature, the domains are instead confined in localized regions.

At higher temperature the weight of random regions increases, and the size of domains is reduced. In this regime, since the density of the potential energy is bounded, most of the energy is kinetic, and therefore most of the spins are fully rotating, with similar amplitudes. This is illustrated in Fig. 9, where the typical temporal behavior of one spin in a high temperature field is shown. Conversely, at low temperatures, angles remain bounded in time. On the other hand, the spin momentum takes essentially constant values (positive or negative ones, depending on the sense of rotation). The individual behavior of the spins also reflects the statistical properties of the system. The angle variance is bounded at low temperatures, in agreement with the random phase approximation, while it steadily increases in time at high temperatures, as we can see in Fig. 10. In analogy with the properties of a perturbed pendulum, the change of the topology of trajectories is related to the crossing of a separatrix. Below a certain value of the energy density h_c [$h_c=h(T_{KT})\approx 1$ in our model], the spins are collectively trapped, and, after the transition, as the behavior of the topological defects suggests, they start to rotate in organized domains, whose size progressively decreases as the energy density increases.

An important consequence of these results is that the system, at these temperatures, can be represented by local ordered regions of synchronized spin motion, and random interfaces where the defects accumulate. To these rotating spin domains, one may add some level of fast (with respect to the

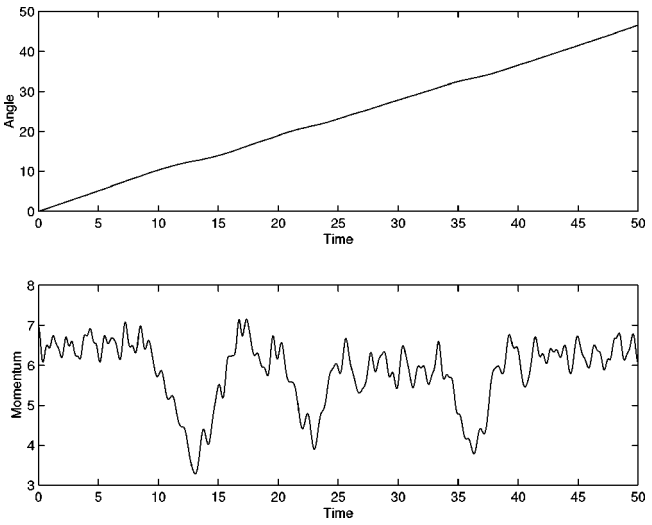

FIG. 9. Typical temporal behavior of a rotator at high temperature. Top: spin $\theta_i(t)$ at the central site for $T=4.100$, measured in units of 2π. The spin rotates in the same direction and with an almost steady speed for long periods of time. Bottom: plot of $\dot{\theta}_i(t)$ showing that its fluctuations are fast compared to the evolution of θ_i.

time scale of rotation) fluctuations characterized by an effective low temperature $\tilde{T}$, which takes into account the potential energy. In this context we may introduce relevant variables s_i, which take the values ± 1 according to the sign of spin rotation $\dot{\theta}_i$. It is important to keep in mind that the system is considered to be in its thermodynamical state, and that the temporal average of spin rotation velocity $\overline{\dot{\theta}_i^2}=T$ is, using ergodicity, independent of the spin site. We can then assume that the angle velocity is of the form $\dot{\theta}_i=\Omega_i \approx s_i\sqrt{T}$, and write

$$\theta_i = s_i \Omega t + \tilde{\theta}_i(t/\epsilon), \tag{4.1}$$

where $\Omega=\sqrt{T}$, and ϵ characterizes the fast temporal fluctuations of the function $\tilde{\theta}_i$, i.e., $|\epsilon| \ll 1$ and $|\tilde{\theta}_i(t/\epsilon)| \ll s_i \Omega t$ (see Fig. 9). The field $\tilde{\theta}_i$ is in fact similar to the θ_i used in Eq. (3.1), but associated with another temperature $\tilde{T}$: in a rotating reference system, attached to each domain (where all the s_i's are equal), it is an effective ''low temperature'' XY spin field.

The introduction of a new field $s_i=\pm 1$, which labels each lattice site by the sign of the spin rotation, suggests an analogy between the high temperature XY system and the Ising model. We will exploit this analogy to construct a model aimed at describing the complex properties of the system near the Kosterlitz-Thouless transition, which do not resume to the simple unbinding mechanism of dipole vortices.

In order to map the XY system into an Ising system, we take advantage of the time scale separation between the relative slow rotation and the fast thermal fluctuations. Let us now average the potential energy over a few rotation periods, during which the approximation made in Eq. (4.1) remains valid. For that purpose, we are reduced to computing the average of terms of the form

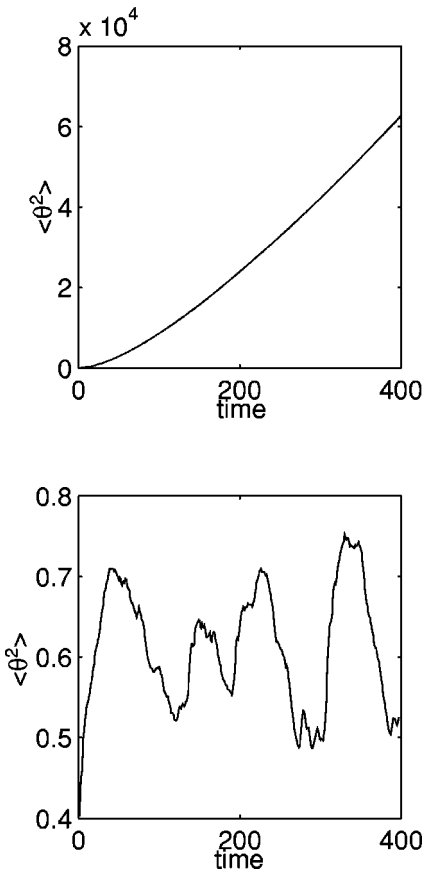

FIG. 10. The spatial variance of θ vs time is plotted for different temperatures. At the bottom we have the plot for $T=0.4783$, while on top the one for $T=2.7905$. The numerical data are obtained for a lattice size of $N=256^2$. We clearly see that the variance of θ is an increasing function of time only for $T>T_{\mathrm{KT}}$.

$$\overline{\cos(\theta_i-\theta_j)} = \overline{\cos[(s_i-s_j)\Omega t]\cos(\tilde{\theta}_i-\tilde{\theta}_j)} - \overline{\sin[(s_i-s_j)\Omega t]\sin(\tilde{\theta}_i-\tilde{\theta}_j)}, \tag{4.2}$$

where i and j denote two neighbors. The fast temporal behavior of the $\tilde{\theta}_i$'s assures its fast thermalization at a temperature $\tilde{T}$, and decorrelates the two terms in each product. This allows us to split the time average in two steps, first on the fast time dependence and then on the slower time scale. The first average leads to

$$\overline{\cos(\tilde{\theta}_i-\tilde{\theta}_j)}=\frac{v(\tilde{T})}{2}, \quad \overline{\sin(\tilde{\theta}_i-\tilde{\theta}_j)}=0,$$

where we use the results of Sec. III, due to the effective low temperature $\tilde{T}$ within a domain. Then the mean of $\cos[(s_i-s_j)\Omega t]$ is zero if the two spins do not rotate in the same direction (do not belong to the same domain), and one if the two spins corotate, which means that the average of this terms can be represented by a Heaviside function $\Theta(s_i s_j)$. We then obtain the expression

$$\overline{v}=\frac{1}{2N}\sum_{\langle i,j\rangle}\overline{\cos(\theta_i-\theta_j)}=\frac{v(\tilde{T})}{4N}\sum_{\langle i,j\rangle}\Theta(s_i s_j) \tag{4.3}$$

for the mean interaction energy, where the summation is over all neighbors, and the Heaviside function just states that only synchronized, corotating spins contribute to the averaged potential energy. Using the identity $\Theta(s_i s_j)=(1+s_i s_j)/2$, we finally obtain an effective Hamiltonian

$$H_e = N\left(\frac{T}{2}+2-\frac{v(\tilde{T})}{2}\right)-\frac{v(\tilde{T})}{4}\sum_{\langle i,j\rangle} s_i s_j . \qquad (4.4)$$

We notice that this effective Hamiltonian is the sum of two different terms, which we denote H_T and H_I. The first term H_T depends on the temperature, the size of the lattice, and $v(\tilde{T})$, and can therefore be considered as an energy reference term. The second term H_I introduces a coupling energy between the spins, and can be recognized as a ferromagnetic Ising-like Hamiltonian whose coupling constant $J_I(T)=v(\tilde{T})/4$ is a function of the temperature. Using an Ising terminology, we now have a population of spins $s_i=\pm 1$, interacting with their close neighbors on a square lattice. Therefore, under the assumption of ergodicity and taking into account that spins rotate on a well separated time scale with respect to their fluctuations, we have mapped the XY system into a Ising-like model; these two models are linked through a coupling constant dependent on a temperature related to fluctuations. We shall note that the time dependence of the Hamiltonian is masked, but the s_i's are still functions of time, and we still are within the microcanonical ensemble. Invoking again the thermodynamical equilibrium, and the fact that both the microcanonial and canonical approaches lead to the same thermodynamic limit, we can now continue our study within the canonical ensemble.

As is well known, the Ising model undergoes a phase transition and generates a spontaneous magnetization M_I when $J_I/T>\beta_{Ic}\approx 0.44$ [24]. In order to know if the present Ising system reaches the transition, we have to investigate the behavior of $v(\tilde{T})$. The previously observed domains (Fig. 8) are in agreement with the phenomenology of the Ising model above its transition, the maximum value of the coupling constant being $v(\tilde{T})/4<\frac{1}{2}$ implies that both models are surely in their high temperature states for $T>1/2\beta_{Ic}\approx 1.14$. In the low temperature regime, none of the spins are rotating; $T=\tilde{T}$ and $v_I=v$, and all the potential energy is due to the waves. We know that the energy is continuous through the Kosterlitz-Thouless transition and also through the Ising transition. As a consequence, we expect that $v(T_{\mathrm{KT}})=v(\tilde{T})$ at the transition temperature. Moreover, the effective domain temperature $\tilde{T}$ has to be an increasing function of T, and then v_I is a decreasing function of T; in order to obtain $h=T/2+2$ at high temperature, $v(\tilde{t})$ has to vanish as $T\to\infty$. The equation

$$J_I/T = v(\tilde{T})/(4T)=\beta_{Ic} \qquad (4.5)$$

therefore has a unique solution. A calculation of T_{KT}, using Eqs. (4.5) and (3.18), gives $T_{\mathrm{KT}}\approx 0.855$, which is in good agreement with the numerical value of $T_{\mathrm{KT}}\approx 0.898$ found in the literature.

There is, however, an important difference between the usual Ising model, and the present one, derived from the XY system. It is the global constraint associated with the conservation of the total momentum. The mean value of the total momentum $P=0$ is given by $0=\Sigma\dot{\theta}_i=\Sigma s_i$. But this last expression is precisely the Ising magnetization

$$M_I=\frac{1}{N}\sum_i s_i = 0, \qquad (4.6)$$

which means that only symmetric distribution of positive and negative spins are allowed. This constraint prevents the system from undergoing, as in the Ising model, a second order phase transition, with the spontaneous appearance of a macroscopic magnetization below the critical temperature. In the present case, this would mean that a significant fraction of the spins would rotate in a preferred direction, but Eq. (4.6) forbids this kind of phase transition, and forces the system to accommodate to a vanishing magnetization. In fact, what happens is that, below the transition temperature, the spins cannot fully rotate, domains disappear, and the long range order is established by a reorganization of spin motions in the form of spin waves, which can still generate a nonintensive finite-size magnetization.

V. CONCLUSION

In this paper we took a dynamical point of view to analyze the statistical properties of the XY model. This approach has the advantage of offering a natural physical framework. From the structure of the evolution equations of the spins (which become coupled oscillators in the linear approximation), one is prompted to consider the phonons (propagating waves in the lattice) as the basic excitation at low temperature. In the thermodynamic limit, and assuming that the system reaches an ergodic equilibrium state, it is reasonable to introduce random phases in the waves. Using this basic mechanism, we obtained a nonlinear dispersion relation containing the fundamental physics of the system. Macroscopic quantities, such as the energy and the (finite size) magnetization, are well described by this method up to temperatures close to the Kosterlitz-Thouless critical temperature.

On the other hand, for high temperatures, our dynamical approach allowed us to map the XY model into an Ising model with a coupling constant depending on the temperature. This relation to an exact model is beneficial to understanding the physics near the transition, and moreover permits an analytical computation of the critical temperature, in excellent agreement with Monte Carlo simulations.

These results lead to a physical description of the Kosterlitz-Thouless transition in terms of the change from an ordered state (long range correlation are established by the wave excitations) to a local ordered state where macroscopic domains are separated by interfaces populated with topological defects. Topological defects have then a tendency to bind themselves in clusters. The generation of disorder by the unbinding of dipoles is accompanied by the fragmentation of

the low energy unique domain of nonrotating spins into separated regions of synchronized rotating spins.

ACKNOWLEDGMENTS

We gratefully acknowledge useful discussions with O. Agullo and D. Benisti. We thank P. C. W. Holdsworth for giving us his Monte Carlo data used in Figs. 1 and 2. Part of the numerical simulations were performed at the Center de Calcul Régional, Région Provence-Alpes-Côte d'Azur. A.V. acknowledges INFM-FORUM for financially supporting his visits to Florence. This work was also part of the EC Network No. ERBCHRX-CT94-0460.

[1] C. Itzykson and J. M. Drouffe, *Théorie Statistique des Champs* (CNRS, Paris, 1989).
[2] M. Le Bellac, *Des Phénomènes Critiques aux Champs de Jauge* (CNRS, Paris, 1988).
[3] V. L. Berezinskii, Zh. Eksp. Teor. Fiz. **59**, 907 (1970) [Sov. Phys. JETP **32**, 493 (1971)].
[4] J. M. Kosterlitz and D. J. Thouless, J. Phys. C **6**, 1181 (1973).
[5] V. L. Berezinskii, and A. Ya. Blank, Zh. Eksp. Teor. Fiz. **64**, 725 (1973) [Sov. Phys. JETP **37**, 369 (1973)].
[6] J. Villain, J. Phys. (Paris) **36**, 581 (1975).
[7] J. M. Kosterlitz, J. Phys. C **7**, 1046 (1974).
[8] P. Minnhagen, Rev. Mod. Phys. **59**, 1001 (1987).
[9] J. Tobochnik and G. V. Chester, Phys. Rev. B **20**, 3761 (1979).
[10] B. Yurke, A. N. Pargellis, T. Kovacs, and D. A. Huse, Phys. Rev. E **47**, 1525 (1993).
[11] P. Olsson, Phys. Rev. Lett. **73**, 3339 (1994).
[12] H. Weber and H. Jeldtoft Jensen, Phys. Rev. B **44**, 454 (1991).
[13] J. Ford, Phys. Rep. **213**, 271 (1992).
[14] D. Escande, H. Kantz, R. Livi, and S. Ruffo, J. Stat. Phys. **76**, 605 (1994).
[15] M. Antoni and S. Ruffo, Phys. Rev. E **52**, 2361 (1995).
[16] L. Casetti, C. Clementi, and M. Pettini, Phys. Rev. E **54**, 5969 (1996).
[17] Ch. Dallago and H. Posch, Physica A **230**, 364 (1996).
[18] P. Butera and G. Caravati, Phys. Rev. A **36**, 962 (1987).
[19] S. T. Bramwell and P. C. W. Holdsworth, Phys. Rev. B **49**, 8811 (1994).
[20] S. T. Bramwell and P. C. W. Holdsworth, J. Phys. Condens. Matter **5**, L53 (1993).
[21] S. Samuel, Phys. Rev. B **25**, 1755 (1982).
[22] D. Spisak, Physica B **190**, 407 (1993).
[23] P. Archambault, S. T. Bramwell, and P. C. W. Holdsworth, J. Phys. A: Math. Gen. **30**, 8363 (1997).
[24] L. Landau and E. Lifschitz, *Physique Statistique* (Ellipses, Paris, 1994).